

Photocatalytic-Fenton Degradation of Glycerol Solution over Visible Light-Responsive CuFe_2O_4

Chin Kui Cheng · Zi Ying Kong · Maksudur R. Khan

Received: 4 May 2015 / Accepted: 28 August 2015 / Published online: 8 September 2015
© Springer International Publishing Switzerland 2015

Abstract The current work reports on the degradation of glycerol aqueous solution via photocatalytic-Fenton technique. The CuFe_2O_4 photocatalyst was synthesized via sol-gel method and its physicochemical properties were characterized. The as-synthesized photocatalyst possessed Brunauer-Emmett-Teller (BET)-specific surface area of $104 \text{ m}^2/\text{g}$. The large BET-specific surface area was also corroborated by the field-emission scanning electron microscopy (FESEM) images which showed porous morphology. In addition, the XRD pattern showed that the visible light-active component, CuFe_2O_4 , was successfully formed with band gap energy of 1.58 eV determined from the UV-Vis diffuse reflectance spectroscopy. Significantly, it was determined from the blank run study that the visible light was an integral part of the photoreaction. Without the visible light irradiation, glycerol degradation was low ($<4.0 \%$). In contrast, when visible light was present, the glycerol degradation improved markedly to attain 17.7% after 4 h of visible light irradiation, even in the absence of CuFe_2O_4 photocatalyst. This can be attributed to splitting of H_2O_2 into hydroxyl ($\bullet\text{OH}$) radical. In

the presence of CuFe_2O_4 photocatalyst, the photocatalytic Fenton degradation of glycerol has further enhanced to record nearly 40.0% degradation at a catalyst loading of 5.0 g/l . This has demonstrated that the CuFe_2O_4 was capable of generating additional hydroxyl radicals to attack the glycerol molecule. Moreover, this degradation kinetics can be captured by Langmuir-Hinshelwood model from which it was found that the adsorption constant related to H_2O_2 was significantly weaker compared to the adsorption constant of glycerol.

Keywords Copper ferrite · Fenton · Glycerol · Langmuir-Hinshelwood · Photocatalysis

1 Introduction

Glycerol is unwittingly produced as a byproduct during the synthesis of biodiesel. According to Yang et al. (2012), production of biodiesel generates 10% w/w glycerol. Traditionally, it is mainly used in food industry, in pharmaceutical and personal care applications, and also as a chemical intermediate (Qadariyah et al. 2011; Yang et al. 2012; Tan et al. 2013; Quispe et al. 2013). Significantly, there is a growing consensus that the biodiesel production will increase in the future; hence, the glycerol production. With the world biodiesel market most likely reaching 37 billion gallons by 2016, this will translate into approximately 4 billion gallons of crude glycerol. If left untreated, this crude glycerol will pose detrimental effects to the environment if discharged into the waterway. Therefore, glycerol

C. K. Cheng · Z. Y. Kong · M. R. Khan
Faculty of Chemical and Natural Resources Engineering,
Universiti Malaysia Pahang, Lebuhraya Tun Razak, Gambang,
26300 Kuantan, Pahang, Malaysia

C. K. Cheng (✉)
Rare Earth Research Centre, Universiti Malaysia Pahang,
Lebuhraya Tun Razak, Gambang, 26300 Kuantan, Pahang,
Malaysia
e-mail: chinkui@ump.edu.my

wastewater requires treatment before being discharged. Interestingly, one of the pathways is via photocatalysis whereby photon energy will be employed to degrade organic contaminants. There are many types of photocatalysts, with the titanium dioxide (TiO_2) being the most well-known material owing to its high photocatalytic activity, good photostability, non-toxicity, and low price (Sharma et al. 2001, 2010; Sharma and Chenay 2005; Eng et al. 2010; Casbeer et al. 2012; Aazam 2014). Unfortunately, TiO_2 -based photocatalyst for commercial application is hampered by two disadvantages, such as the agglomeration of ultrafine powders resulting in an adverse effect on catalyst performance (Aazam 2014) and also the wide band gap energy (>3.1 eV) that restricts its photocatalytic application to the UV zone (200 to 400 nm). The UV zone accounts for a meager 4 % of the solar energy spectrum. Consequently, it results in low photoelectronic transition efficiency (Casbeer et al. 2012; Shahid et al. 2013). Significantly, efforts are ongoing to develop new breeds of photocatalysts that can function under wider range of light illumination, i.e., visible light. In particular, various non-titania photocatalysts were developed recently for dyes degradation, viz. BiOX ($X = \text{Cl}, \text{F}, \text{Br}, \text{I}$) (Vadivel et al. 2014), Ni-doped Ag_2S (Aazam 2014), $\text{Ag}_3\text{PO}_4\text{-AgX}$ ($X = \text{Cl}^-, \text{Br}^-, \text{I}^-$) (Amornpitoksuk and Suwanboon 2014), BiVO_4 (Chala et al. 2014), to name a few.

Ferrite-based catalyst is also another class of catalyst that can function under the visible light (400 to 700 nm). Hence, copper ferrite (CuFe_2O_4) was employed for this work. For the past few years, researchers have conducted some research works on CuFe_2O_4 utilization in advanced oxidation processes (AOPs) or photocatalytic degradation of glycerol, such as the one by Yang et al. (2009), Melo and Silva (2011), Ghomi and Ashayeri (2012), Shen et al. (2013), Zhu et al. (2013) and Liu et al. (2014), to name a few. Nevertheless, these prior studies focused either on the CuFe_2O_4 photocatalyst characterization or photodecomposition of glycerol employing titania-based photocatalysts. Furthermore, studies regarding Fenton degradation of glycerol was also very limited, and was reported before by Laurie and Waterhouse (2006). To date, the use of CuFe_2O_4 to photocatalytic degrade glycerol in the presence of H_2O_2 , coined as photocatalytic Fenton-alike process, has not been investigated. Therefore, significant knowledge gap can be found concerning the understanding of glycerol photodecomposition over the CuFe_2O_4 photocatalyst.

In this study, CuFe_2O_4 was prepared using sol-gel method as it is a superior method compared to the solid-solid and co-precipitation methods (Yang et al. 2009). The CuFe_2O_4 was characterized by x-ray diffraction (XRD), field-emission scanning electron microscopy-energy dispersive x-ray analysis (FESEM-EDX), UV-Vis diffuse reflectance spectroscopy (DRS) and N_2 physisorption methods. Subsequently, CuFe_2O_4 photocatalyst was employed in the photocatalytic Fenton degradation of glycerol for investigation of the effects of different catalyst loadings, as well as different concentration of glycerol solution and hydrogen peroxide (H_2O_2).

2 Experimental

2.1 Chemical and Materials

Copper (II) nitrate trihydrate, iron (III) nitrate nonahydrate, citric acid, and glycerol were purchased from Sigma Aldrich. Hydrogen peroxide (30 %) was sourced from Merck while acetonitrile (HPLC grade) was from Fischer Chemical. All the chemicals were used as received.

2.2 CuFe_2O_4 Photocatalyst Synthesis

The CuFe_2O_4 photocatalyst was prepared using sol-gel method. Accurately weighed 0.005 mol $\text{Cu}(\text{NO}_3)_2 \cdot 3\text{H}_2\text{O}$ and 0.01 mol $\text{Fe}(\text{NO}_3)_3 \cdot 9\text{H}_2\text{O}$ were co-dissolved in 50-ml distilled water. The mixed solution was subsequently added into 100 ml of 0.3-M citric acid solution. During the mixing, the temperature of solution was controlled at 80 °C until transparent and viscous gel was obtained. The gel was subsequently transferred into an oven and dried at 140 °C for 3 h. The as-prepared precursors were then air-calcined at 850 °C for 3 h at a ramping rate of 10 °C min^{-1} . The calcined catalyst was then ground and stored in the vials for catalyst characterization and photocatalytic Fenton study.

2.3 Characterization of CuFe_2O_4

The as-synthesized photocatalyst was subjected to a series of characterization. N_2 with a cross-sectional area of 0.162 nm^2 was used as an adsorbate for adsorption-desorption cycles performed at 77 K in a Thermo

Scientific Surfer Gas Adsorption Porosimeter for the determination of specific surface area. The crystallinity of the catalyst was examined using the Rigaku Miniflex II. The XRD measurement had employed CuK_α radiation, $\lambda=1.5418\text{\AA}$ at 30 kV and 15 mA, with 2θ from 10 to 80° with a step size of 0.02° and a step time of 1 s. The crystal size of the catalyst was subsequently determined from the Scherrer equation $d = \frac{0.94 \times \lambda}{\beta_d \cos \theta}$, where d is the crystallite size, λ is the wavelength of the radiation, β_d is the full width at half maximum (FWHM) of the diffraction peak, and θ is the half of the diffraction angle. In addition, the surface morphology of the catalyst was captured using the JEOL JSM-7800 F (FESEM-EDX) at 3–5 kV.

2.4 Photocatalytic Fenton Activity

For the reaction study, 200 ml of reaction media was mixed with photocatalyst in a quartz-photoreactor. Subsequently, the slurry mixture was stirred rigorously for 30 min (without light source) to attain equilibrium, followed by the exposure to light source (250 W of xenon lamp) for reaction initiation. Approximately 5.0 ml of liquid sample was collected every 1 h for analysis. All the photocatalytic Fenton runs were repeated thrice and results obtained were then averaged. Overall, three types of effects have been investigated, viz. (i) the effects of photocatalyst loadings (0.1, 1.0, 2.0 and 5.0 g/l) on glycerol degradation at 68.4 mM of glycerol and 819.5 mM of H_2O_2 ; (ii) the effects of initial glycerol concentration on glycerol photocatalytic Fenton decomposition whereby the initial glycerol concentration was varied from 27.36 to 68.41 mM in the presence of 0.1 g/l of CuFe_2O_4 and 819.5 mM H_2O_2 ; and also (iii) the effects of H_2O_2 concentration (163.9 to 819.5 mM) on glycerol degradation were conducted at 0.1 g/l CuFe_2O_4 .

2.5 Sample Analysis

Quantitative sample analysis was performed using Agilent 1200 Series HPLC equipped with refractive index (RI) detector. The column used in this study was Agilent ZORBAX Carbohydrate 5- μm column (inner diameter of 4.6 and length of 250 mm) with the flow rate of 1.0 ml/min and injection volume of 10 μm . The mobile phase used throughout the HPLC analysis was acetonitrile (ACN) diluted with ultrapure water in a ratio

of 7:3. Prior to the HPLC analysis, the mobile phase was filtered using nylon membrane with a pore size of 0.2 μm and then degassed using ultrasonic bath at room temperature for 30 min. Standard calibration to determine concentration of reactants was carried out for both glycerol and H_2O_2 employing the aforementioned HPLC, whereby the H_2O_2 peak was detected at a retention time of 3.93 min while glycerol's peak was detected at 4.6 min. The degree of photodegradation (X) as a function of time is given by:

$$X = \frac{C_{A0} - C_A}{C_{A0}} \quad (1)$$

where C_{A0} is the glycerol or H_2O_2 's initial concentration while C_A is the instantaneous concentration of glycerol or H_2O_2 .

3 Results and Discussion

3.1 N_2 Physisorption

The N_2 physisorption isotherm of CuFe_2O_4 is shown in Fig. 1 whereby the plot provides the information regarding textural properties of CuFe_2O_4 . The value of the pore volume was taken at $P/P^0=0.95$. The two curves in the isotherm plot are representation of adsorption and desorption of N_2 molecules on the CuFe_2O_4 solid sample. At low-pressure range, the N_2 molecules began to fill the pores of the CuFe_2O_4 rapidly, and this was manifested by its steep slope with pressure increment at the onset. As the pressure continued to increase, the surface pores were eventually covered by N_2 . The amount of N_2 molecules adsorbed was therefore not so influenced by the increase in pressure. This occurred in the middle phase of the isotherm. Brunauer-Emmett-Teller (BET) isotherm applies the assumption that all sites on the sample surface are equivalent. However, deviation occurred at high pressures due to the presence of cracks and indents. These types of surfaces can only hold a few monolayers of nitrogen at lower pressures. High pressure forces the adsorption of nitrogen to form multi-layers; thus, the curve turned steep at the end of the isotherm (cf. Fig. 1). Moreover, it can be observed that the adsorption and desorption curves have deviated to form hysteresis loop. Generally, adsorption of an equilibrium amount of adsorbate is a reversible process, resulting in a same curve for adsorption and desorption.

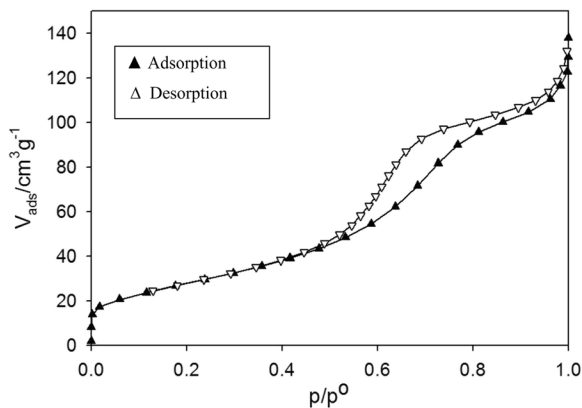


Fig. 1 Isotherm of CuFe_2O_4 from N_2 physisorption analysis

However, in the case of curved surfaces, such as the mesoporous surface in this case, the amount of N_2 molecules adsorbed upon increasing or decreasing the gas pressure, did not coincide over a certain interval of pressures. The capillary condensation is a phenomenon of liquid-gas phase transitions under porous confinement which explains the resulting hysteresis loop. This hysteresis phenomenon showed that the pores on the samples were mesoporous in nature. For the purpose of specific surface area determination, the 2-parameter line model showed the highest regression consequently, the estimated BET-specific surface area of the synthesized CuFe_2O_4 in the current work was $102.4 \text{ m}^2/\text{g}$. In addition, the BJH cumulative pore volume was estimated at $0.1866 \text{ cm}^3/\text{g}$ while the average pore diameter was found to be 52.67 \AA .

3.2 FESEM-EDX Analysis

The FESEM-EDX technique was employed in the current work to examine both the morphology as well as element identifications of fresh CuFe_2O_4 (cf. Fig. 2). The morphology of the CuFe_2O_4 at different level of magnifications, viz. $\times 5000$; $\times 20,000$; and $\times 50,000$, showed solid specimen with irregularly shaped nanoparticles, albeit with good homogeneity in particle size distribution. Moreover, the particles also appeared fused together, which may be attributed to the high calcination temperature ($850 \text{ }^\circ\text{C}$) employed in this study. Furthermore, it can be observed that the structure was porous with formation of noticeable void volume, consistent with large BET-specific surface area obtained from the N_2 physisorption analysis as aforementioned.

The EDX spectrum taken on the same CuFe_2O_4 photocatalyst showed that the solid was indeed comprised of Cu, Fe, and O elements only, unadulterated by other impurities. The element C detected was attributed to the background.

3.3 XRD Analysis

X-ray diffraction (XRD) was used to determine the crystal phase of the photocatalyst. Figure 3 shows the XRD pattern of the CuFe_2O_4 photocatalyst. The sharp diffracted peaks were an indication of well-defined crystallite structure. Significantly, a new visible light-active compound known as the copper ferrite (CuFe_2O_4) crystal was detected. Therefore, it can be surmised that the catalyst formulation and synthesis strategy has successfully produced the desired solid phase. This result was also consistent with the EDX analysis in Section 3.2. Copper ferrite is a member of the magnetite series of spinel with 2θ of 18.56 , 30.08 , 34.82 , 36.03 , 37.27 , 54.23 , and 62.25 $^\circ$. It takes the form of cubic with lattice parameters $a=5.82 \text{ \AA}$, $b=5.82 \text{ \AA}$, and $c=8.62 \text{ \AA}$. The average crystallite sizes which was calculated using the Scherrer equation showed that the crystallite sizes of CuFe_2O_4 were ranged from 5.0 to 90.0 nm as summarized in Table 1. Traces of Fe_2O_3 and CuO are also visible, recorded at 2θ of 32.0 and 39.0 $^\circ$, respectively.

3.4 Optical Properties

Figure 4 shows the UV-Vis DRS spectrum of CuFe_2O_4 . From the figure, it can be estimated that the minimum wavelength required for the prepared CuFe_2O_4 photocatalyst to be active was 785 nm or in other words, the CuFe_2O_4 was active under visible light irradiation of wavelength up to 785 nm . The energy required by photon to generate electron-hole pair in a photocatalyst can be related to its wavelength (Wade 2005) by the equation $E_{bg} = \frac{1240}{\lambda}$, where λ is the wavelength of photon in nanometers and E_{bg} is the band gap of semiconductor in electronvolts. The band gap of the as-synthesized CuFe_2O_4 was obtained by plotting data from UV-Vis and was found to be 1.58 eV . The band gap energy magnitude showed that the prepared CuFe_2O_4 has a larger band gap than the one reported by Derbal et al. (2008) with a band gap of 1.32 eV . This could be due to the presence of some CuO (1.6 eV)

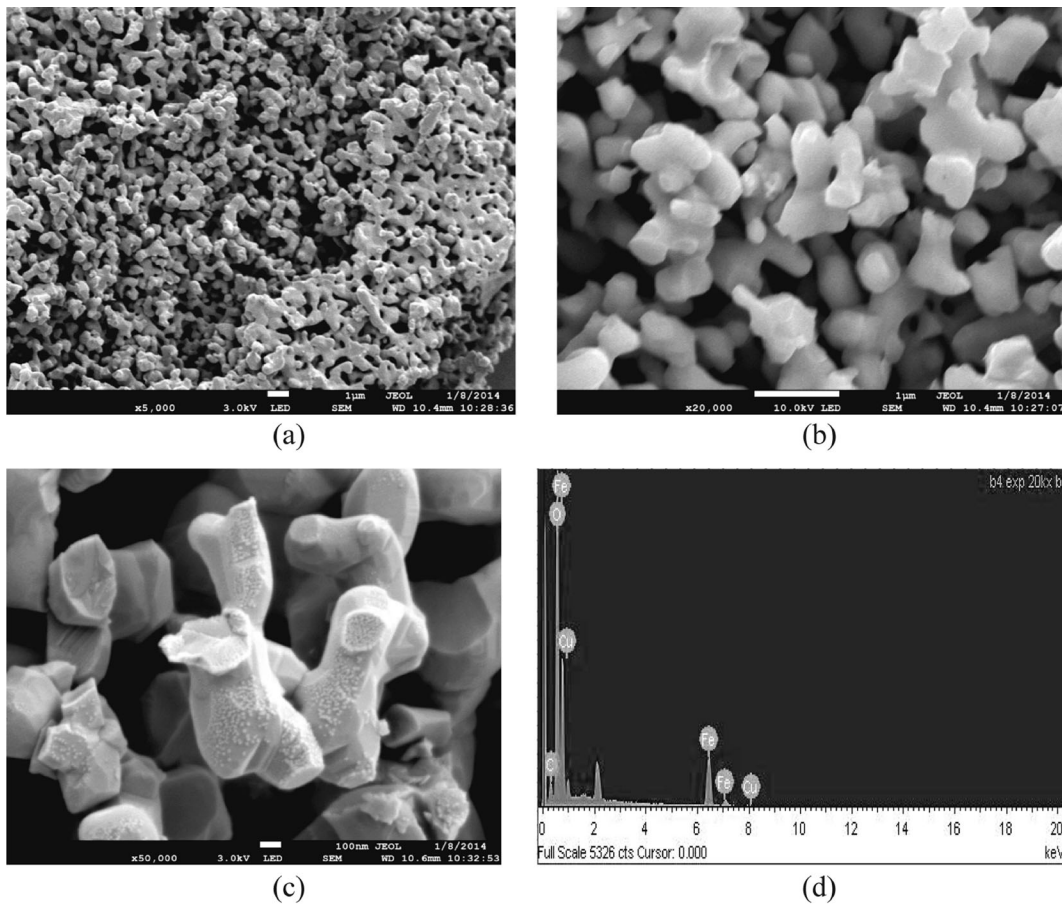


Fig. 2 a–c FESEM image of the fresh CuFe_2O_4 at different magnification levels. **d** EDX image of the fresh CuFe_2O_4 photocatalyst

(Kumar et al. 2013) and Fe_2O_3 (2.2 eV) (Blake 1999) impurity phase as evinced in the XRD diffractogram (cf. Fig. 3).

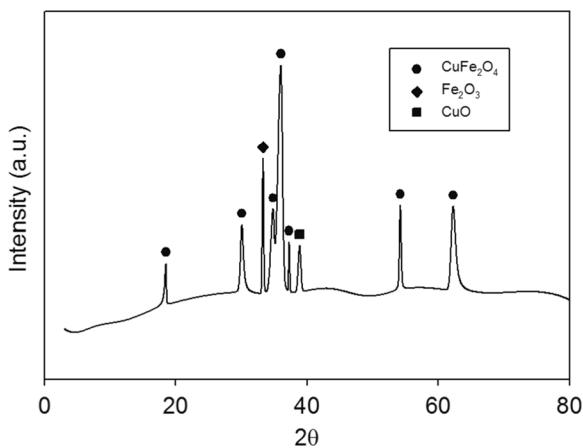


Fig. 3 XRD pattern of CuFe_2O_4 solid sample

3.5 Photocatalytic Fenton Activity Evaluation

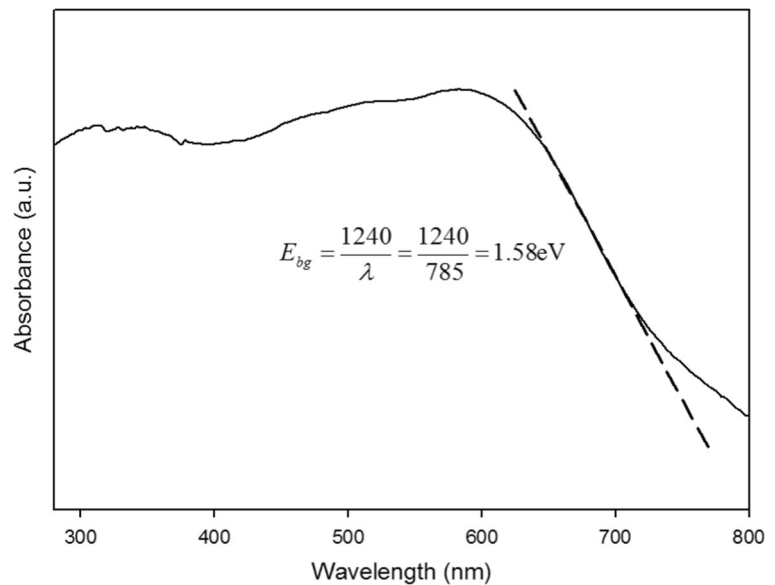
3.5.1 Adsorption and Direct Photolysis Studies

Adsorption study was carried out to determine both the glycerol and H_2O_2 uptakes by the CuFe_2O_4 at room temperature. In the current study, the adsorption run was carried out at a loading of 0.1 g/l CuFe_2O_4 photocatalyst and reactant concentrations that were

Table 1 Summary of crystal phase and its corresponding size

2θ (°)	Phase name	Crystallite size (nm)
18.56	Copper ferrite (1 0 1)	88
30.08	Copper ferrite (1 1 2)	14
34.82	Copper ferrite (1 0 3)	11
36.03	Copper ferrite (2 1 1)	5
54.23	Copper ferrite (3 0 2)	90
62.25	Copper ferrite (2 2 4)	9

Fig. 4 Graph of absorbance versus wavelength for as-synthesized CuFe_2O_4



comprised of 68.41-mM glycerol and 819.5 mM of H_2O_2 . Without light irradiation, the glycerol concentration only dropped slightly over the course of 4 h, which corresponds to less than 4.0 % (transient profile not shown). Similar trend was also exhibited by the transient H_2O_2 concentration result which demonstrated an average loss of just 2.0 % compared to its initial concentration level. It can therefore be surmised that adsorption of both reactants on the CuFe_2O_4 was quite low.

For direct photolysis study (light irradiation only), the 68.41-mM glycerol solution was irradiated with visible light without the presence of H_2O_2 and CuFe_2O_4 photocatalyst. It was found that the glycerol did not degrade, and the initial concentration was still retained even after 4 h of irradiation. Hence, the effect of direct photolysis can be neglected.

3.5.2 Effects of Initial Catalyst Loading

Experiments for determination of the effect of initial catalyst loading were carried out at 68.4 mM of glycerol and 819.5 mM of H_2O_2 . The lower boundary limit of catalyst loadings was set at 0.1 g/l, as loading below this threshold was practically difficult to handle. All the experiment runs were under 250 W of visible light irradiation.

Figures 5 and 6 show the transient concentration profiles of glycerol and H_2O_2 and their transient

conversion, respectively. The concentration profiles of both glycerol and H_2O_2 (refers to Figs. 5a and 6a) show a significant downward trend, symptomatic of progressive chemical reaction. The blank run (without catalyst) indicates that photolysis (combination of H_2O_2 and light only) reaction occurred and achieved glycerol degradation of 17.7 % (cf. Fig. 5) and H_2O_2 utilization of 8.0 % (cf. Fig. 6) after 4 h of reaction. In the presence of CuFe_2O_4 photocatalyst, the onset of photocatalytic Fenton reaction has increased the degradation of glycerol substantially, i.e., at 0.1 g/l of photocatalyst loading, the degradation of glycerol can attain 27.0 % and peaked at almost 40.0 % of glycerol degradation when 5.0 g/l of CuFe_2O_4 photocatalyst loading was employed. By increasing the photocatalyst loadings from 0.1 to 5.0 g/l, the number of active sites would have increase in tandem. Consequently, the glycerol degradation also increased. Indeed, as can be seen in Fig. 5b, the glycerol degradation percentage has incrementally increased with the catalyst loading. This was exhibited by 38.0 % (5.0 g/l) > 36.0 % (2.0 g/l) > 30.0 % (1.0 g/l) > 27.0 % (0.1 g/l).

As aforementioned, H_2O_2 concentration profile as in Fig. 6 also dropped with reaction time, similar to the trend exhibited by the glycerol concentration. The highest H_2O_2 consumption was recorded for the 5.0 g/l (35.0 %) while it was 22.0 % utilization for the CuFe_2O_4 loading of 0.1 g/l which was an impressive result,

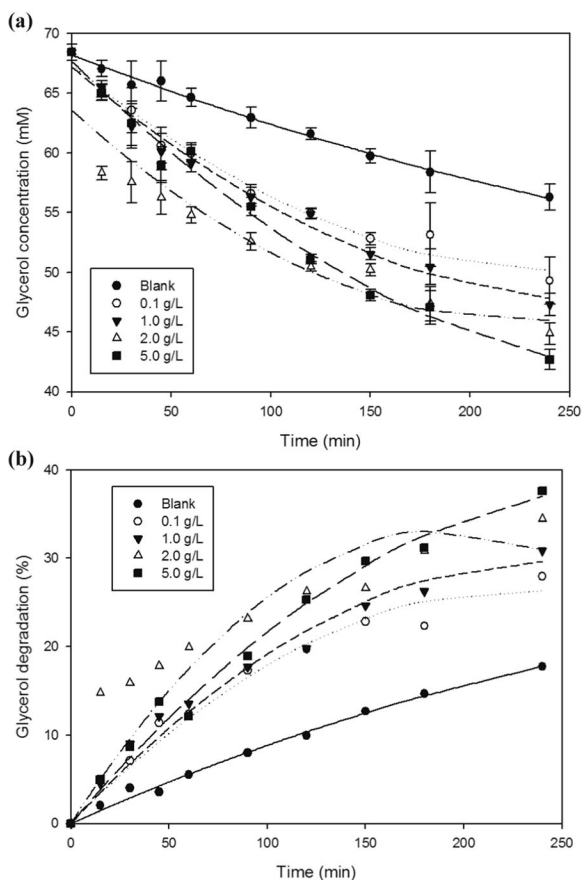


Fig. 5 Transient profiles of **a** glycerol concentration and **b** glycerol degradation (%) at different photocatalyst loadings with 68.41 mM glycerol and 819.5 mM H₂O₂

considering that it only involved a small amount of catalyst. Although the results from the variations in initial photocatalyst loading showed that 5.0 g/l consistently yielded highest utilization of both reactants, a minimum 0.1 g/l of CuFe₂O₄ photocatalyst also gave significant consumption, hence was chosen as the preferred loading for the subsequent investigations.

The results shown in Fig. 5 also demonstrated that the photocatalytic degradation rate has a non-linear dependency on catalyst loading with the maximum occurred at 5.0 g/l. In fact, at high catalyst loadings (2.0 and 5.0 g/L), the effective light intensity has obviously diminished because of the increased solution opacity. The results in Fig. 5 was further regressed and differentiated using Polymath software[®] to obtain the glycerol decomposition rate, $\left(-\frac{dC_{\text{glycerol}}}{dt}\right)$. As the reaction duration was relatively short (240 min) and the reaction may be accompanied by deactivation of catalyst, the method

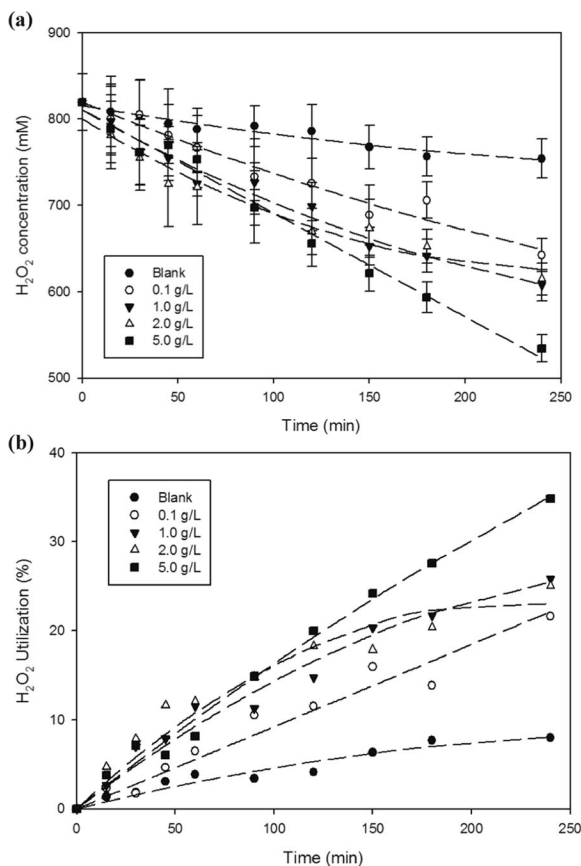


Fig. 6 Transient profiles of **a** H₂O₂ concentration and **b** H₂O₂ utilization at different photocatalyst loadings with 68.41 mM glycerol and 819.5 mM H₂O₂

of initial reaction rate was employed (Fogler 2005). It was found that the reaction rate may be presented by an empirical equation, written as

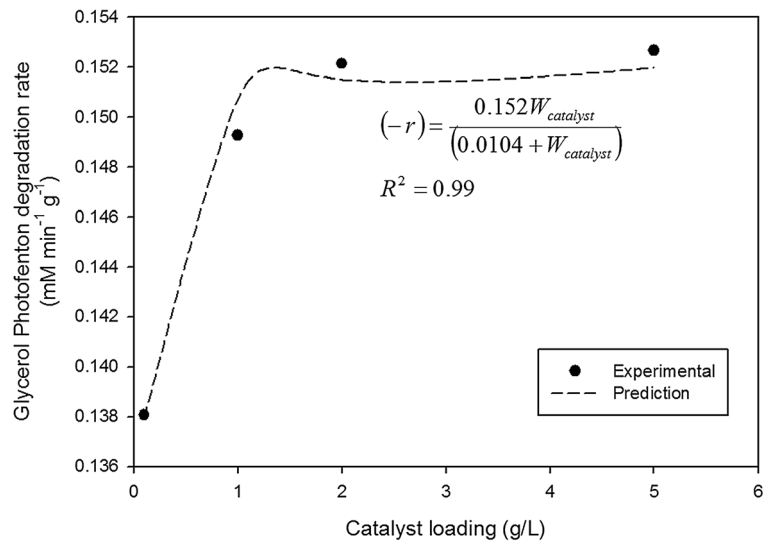
$$(-r_{\text{glycerol}}) = \left(-\frac{dC_{\text{glycerol}}}{dt}\right) = \frac{kW_{\text{catalyst}}}{(\alpha + W_{\text{catalyst}})^2} \quad (2)$$

where W_{catalyst} is the catalyst weight per unit volume of solution, k is a pseudo-rate constant for the catalyst loading, regressed as 0.152 mM min⁻¹, and α is a parameter that indicates volumetric light shielding effect, valuing at 0.0104 g_{cat}/l with a correlation coefficient R^2 of 0.99 (refers to Fig. 7). The unity denominator in the Langmuir-Hinshelwood type of equation indicates the particle-particle interaction.

3.5.3 Effects of Initial Concentration of Glycerol

The investigation of reactant concentration on the kinetics of photocatalytic Fenton degradation of glycerol was

Fig. 7 Glycerol photocatalytic Fenton degradation rate at different photocatalyst loadings



carried out to examine the glycerol conversion. In order to study the effects of initial glycerol concentration on glycerol decomposition, the initial concentration was varied from 27.36 to 68.41 mM in the presence of 0.1 g/l of CuFe_2O_4 and 819.5 mM H_2O_2 . As aforementioned, loading of 0.1 g/L was chosen instead of the other catalyst loadings as this minimum loading was able to yield significant reaction rates.

As shown in Fig. 8a, all the transient concentration profiles exhibit non-linear downward trend. However, by increasing the initial glycerol concentration, the glycerol degradation has decreased (refers to Fig. 8b). Indeed, at 27.36-mM initial glycerol concentration, degradation rate was nearly 60.0 %. In contrast, when the initial glycerol concentration was 68.41 mM, the degradation has dipped to *circa* 30.0 % only. The concentration profiles of H_2O_2 that correspond to the Fig. 8 is presented in Fig. 9 and exhibits similar downward trend indicating that photocatalytic Fenton reaction of glycerol has indeed occurred (simultaneous consumption of both glycerol and H_2O_2). This serves to confirm that H_2O_2 indeed directly partake in the reaction.

3.5.4 Effects of Initial H_2O_2 Concentration

Initial H_2O_2 concentration would also affect glycerol decomposition. Therefore, the effects of H_2O_2 concentration from 163.9 to 819.5 mM has been studied at a constant 68.4-mM glycerol concentration and at a loading of 0.1 g/l CuFe_2O_4 as shown in Figs. 10 and 11. Increasing the H_2O_2 concentration would produce more

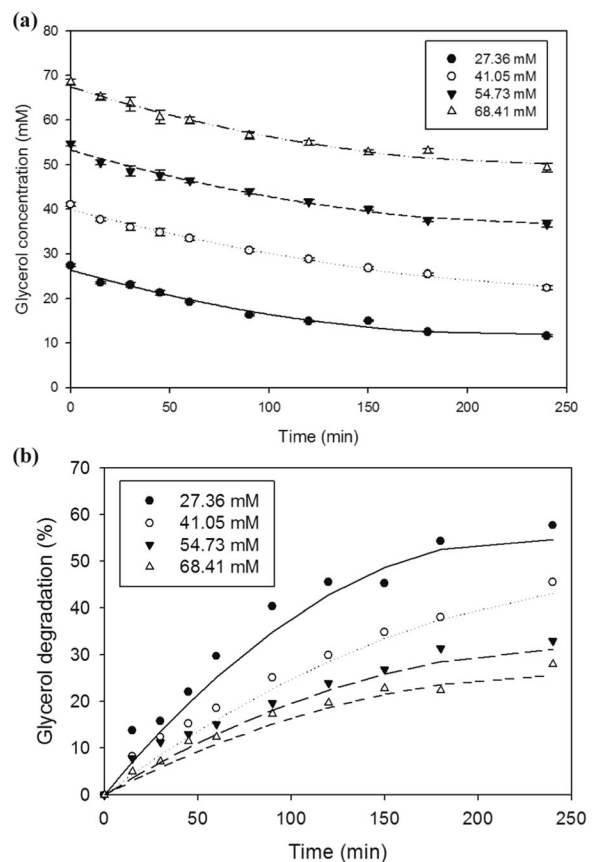


Fig. 8 Transient profiles of **a** glycerol concentration and **b** glycerol degradation (%) at different initial glycerol concentrations and 0.1 g/l CuFe_2O_4

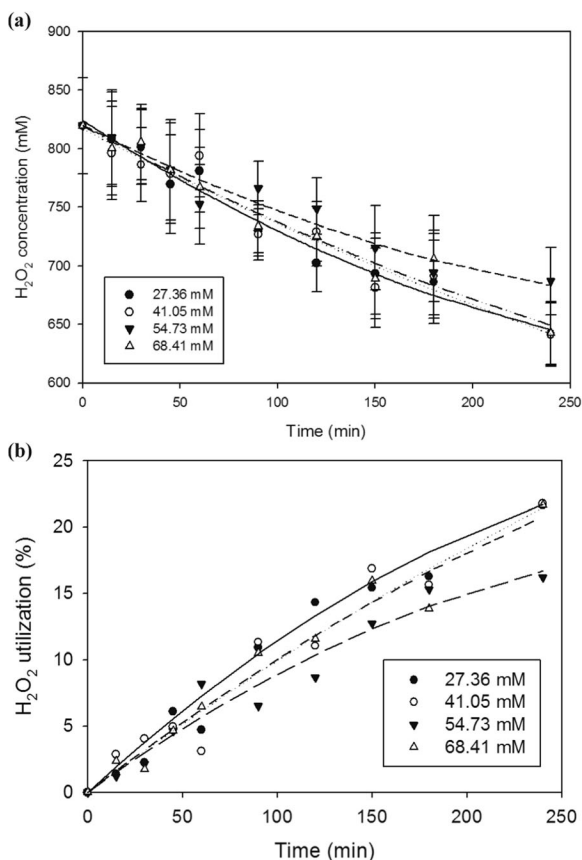


Fig. 9 Transient profiles of **a** H₂O₂ concentration and **b** H₂O₂ utilization (%) at different initial glycerol concentrations and 0.1 g/l CuFe₂O₄

•OH radicals and consequently increase the degradation rate of glycerol. At 163.9-mM initial H₂O₂ concentration, the degradation rate was 5.0 %. By increasing the initial H₂O₂ concentration from 163.9 to 819.5 mM, the degradation rate also increased from 5.0 to 25.0 %.

3.5.5 Power Law Modeling

The results obtained from the variation of initial reactant concentrations demonstrated that the concentration of both C₃H₈O₃ and H₂O₂ affected the rate of photocatalytic Fenton degradation of glycerol. When the transient concentration data were subjected to non-linear regression, followed by finite differentiation of the regression equations, the initial rate of glycerol decomposition was obtained by setting reaction time, *t*=0 min. The values obtained are summarized in Table 2.

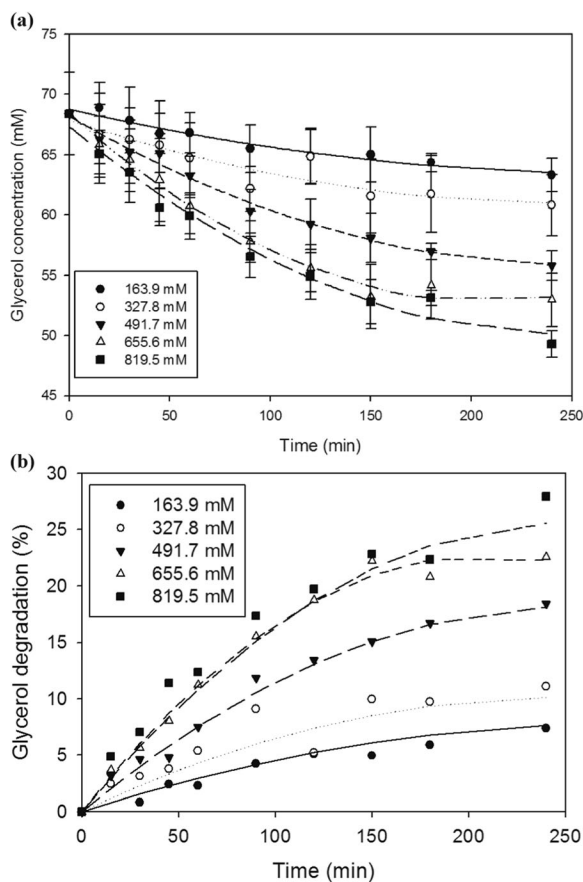


Fig. 10 Transient profiles of **a** glycerol concentration and **b** glycerol degradation (%) at different initial H₂O₂ concentrations and 0.1 g/l CuFe₂O₄

Accordingly, the initial rate of photocatalytic Fenton degradation of glycerol can be described by power law model which takes the form of:

$$(-r_{\text{glycerol}}^o) = k_{\text{app}} C_{\text{glycerol}}^\alpha C_{\text{H}_2\text{O}_2}^\beta \tag{3}$$

where

- (-*r*_{glycerol}^o) Initial rate of glycerol photocatalytic Fenton degradation
- k*_{app} Apparent specific reaction rate (min⁻¹)
- C*_{glycerol} and *C*_{H₂O₂} reactants' initial concentration
- α and β the orders of reaction

A non-linear regression of the initial rate data collected over different reactant concentrations was performed using Polymath software built-in with Levenberg-Marquardt optimization method. The resulting parameter estimates are provided in Table 3 with reasonably excellent adherence to the Power Law

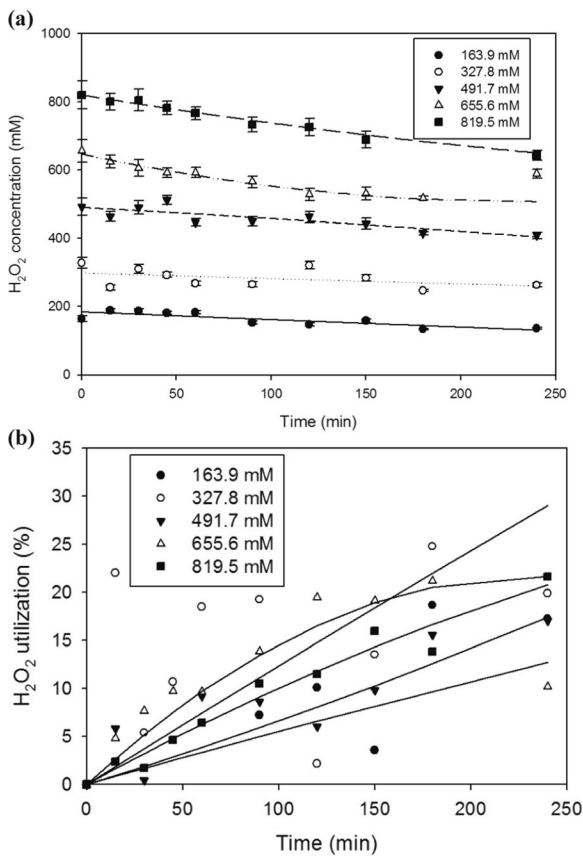


Fig. 11 Transient profiles of **a** H_2O_2 concentration and **b** H_2O_2 utilization (%) at different initial H_2O_2 concentrations and 0.1 g/l CuFe_2O_4

Model judging by the regression co-efficient R^2 of 0.94. Significantly, the order of reactions were fractional, typical characteristic of chemical reaction system, with

Table 2 Summary of initial rate of glycerol degradation computed from the differentiation of transient concentration profiles of glycerol

C_{glycerol} (mM)	$C_{\text{H}_2\text{O}_2}$ (mM)	$-r'_{\text{glycerol}}$ (mM min $^{-1}$)
0	0	0
68.4	163.9	0.0380989
68.4	327.8	0.0551275
68.4	491.7	0.0971941
68.4	655.6	0.1487462
68.4	819.5	0.1380215
27.35	819.5	0.1278486
41.05	819.5	0.11808
54.73	819.5	0.13011

Table 3 Estimates of kinetic parameters from power law equation

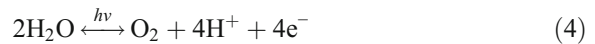
Variable	Value	95 % confidence	R^2
k_{app} (min $^{-1}$)	2.78×10^{-4}	6.78×10^{-5}	
α	0.198734	0.060	0.94
β	0.805445	0.037	

order of reactions associated with H_2O_2 (0.80) was fourfold higher than the order of reaction with respect to glycerol (0.20). This confirmed that H_2O_2 was playing a major role in degrading the glycerol.

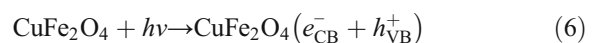
3.5.6 Mechanisms of Photocatalytic Fenton Degradation of Glycerol

From the kinetics trends observed in Figs. 9 to 10, the mechanism of photocatalytic Fenton degradation of glycerol is proposed as follows:

One of the chemical pathways to produce $\bullet\text{OH}$ radicals is as shown in Eqs. (4) to (5):



The steps in (4) and (5) to generate hydroxyl radical were occurring in the homogeneous phase. Indeed, as shown in the blank runs in Section 3.5.2 (without the presence of CuFe_2O_4 photocatalyst or otherwise known as photolysis), reactions in (4) and (5) indeed has occurred in the presence of H_2O_2 and visible light. This also describes the degradation of glycerol and consumption of H_2O_2 under the visible light irradiation without the presence of CuFe_2O_4 . Nonetheless, since the glycerol degradation percentage was substantially lower compared to the results obtained for the cases that involved loadings of CuFe_2O_4 , it can therefore be concluded that in the presence of CuFe_2O_4 , the CuFe_2O_4 photocatalyst has also concurrently absorbed light energy during the irradiation to produce electron-hole pair (Shahid et al. 2013) at the photocatalyst surface as shown in Eq. (6).



Subsequently, more hydroxyl radical ($\bullet\text{OH}$) was generated from H_2O_2 (as in Eq. (5)) via the additional electron from the CuFe_2O_4 (cf. Eq. (6)), and to some extent, albeit minor, via the water molecules breakdown

(Eq. (8)) and also through reaction between hydroxyl ion (OH^-) and hole (cf. Eq. (9)).



The final step would involve the attack of adsorbed glycerol substrate by the $\cdot\text{OH}$ radicals, most likely would mineralize it into simple molecules such as CO_2 and H_2 .

Based on the outlined photocatalytic Fenton mechanisms, the Langmuir-Hinshelwood (LH) model as shown in Eq. (10) can be employed to model the initial rate data as summarized in Table 2.

$$\left(-r_{\text{glycerol}}^o\right) = \frac{k_{\text{rxn}} C_{\text{glycerol}} C_{\text{H}_2\text{O}_2}}{1 + K_{\text{glycerol}} C_{\text{glycerol}} + K_{\text{H}_2\text{O}_2} C_{\text{H}_2\text{O}_2}} \quad (10)$$

where

k_{rxn}	Reaction rate constant ($\text{mM}^{-1} \text{min}^{-1}$)
K_{glycerol}	Adsorption constant for glycerol (mM^{-1})
$K_{\text{H}_2\text{O}_2}$	Adsorption constant for H_2O_2 (mM^{-1})

Once again, a non-linear regression of the initial rate data was performed using Polymath software built-in with Levenberg-Marquardt optimization method. The resulting parameter estimates are provided in Table 4 with reasonably excellent adherence to the LH model ($R^2=0.93$). The glycerol adsorption constant (K_{glycerol}) was 1.010 mM^{-1} , which was larger than the adsorption constant belonging to the H_2O_2 reactant (0.033 mM^{-1}). This indicates that glycerol was chemisorbed onto the surface of CuFe_2O_4 before being attacked by the hydroxyl radical, while the H_2O_2 was predominantly present in the glycerol solution due to the much weaker chemisorption magnitude. Significantly, this is

Table 4 Estimates of kinetic parameters in Eq. (10)

Variable	Value	95 % confidence	R^2
k_{rxn} ($\text{mM}^{-1} \text{min}^{-1}$)	2.60×10^{-4}	6.78×10^{-5}	
K_{glycerol} (mM^{-1})	1.010	0.0015	0.93
$K_{\text{H}_2\text{O}_2}$ (mM^{-1})	0.033	1.13×10^{-4}	

consistent with the mechanisms in (4) to (9) which posit that the breaking of H_2O_2 occurred without the need for the H_2O_2 to chemisorb.

4 Conclusions

The photocatalytic Fenton degradation of glycerol was studied in the current work. It was determined from the blank runs that visible light was an integral part of the reaction. Without the visible light irradiation, glycerol loss was low (<4.0 %). In contrast, when visible light was present, the glycerol degradation improved markedly to attain 17.7 % after 4 h of visible light irradiation in the absence of CuFe_2O_4 photocatalyst. This can be attributed to the two-step splitting of H_2O_2 into hydroxyl ($\cdot\text{OH}$) radical. In the presence of CuFe_2O_4 photocatalyst, the photocatalytic Fenton degradation of glycerol improved substantially to record nearly 40.0 % degradation at a catalyst loading of 5.0 g/L. This has demonstrated that the CuFe_2O_4 under the visible light was capable of generating additional hydroxyl radicals to attack the glycerol molecule. For the effects of initial concentration of reactants, it was found that the initial degradation rate of glycerol can be captured using both power law modeling, as well as Langmuir-Hinshelwood. Significantly, from the power law modeling, the order of reaction with respect to the glycerol (0.20) and H_2O_2 (0.80) was found to be fractional, typical representation of chemical kinetics expression. Furthermore, via the Langmuir-Hinshelwood model, adsorption constant related to H_2O_2 ($0.033 \text{ mM}^{-1} \text{min}^{-1}$) was found to be much weaker compared to the adsorption constant of glycerol ($1.010 \text{ mM}^{-1} \text{min}^{-1}$). This indicates that the H_2O_2 splitting into hydroxyl radical occurred in the bulk phase while the glycerol substrate needs to chemisorb on the catalyst surface before being attacked by the hydroxyl radicals.

Acknowledgments The authors would like to thank the Ministry of Education, Malaysia for the ERGS fund (RDU120613). Zi Ying Kong is thankful to Universiti Malaysia Pahang for providing a studentship (GRS140333).

References

- Aazam, E. S. (2014). Photocatalytic oxidation of methylene blue under visible light by Ni doped Ag_2S nanoparticles. *Journal of Industrial and Engineering Chemistry*, 20(6), 4033–4038.

- Amornpitoksuk, P., & Suwanboon, S. (2014). Photocatalytic decolorization of methylene blue dye by $\text{Ag}_3\text{PO}_4\text{-AgX}$ ($\text{X} = \text{Cl}^-$, Br^- and I^-) under visible light. *Advanced Powder Technology*, 25(3), 1026–1030.
- Blake, D. (1999). *Bibliography of work on the heterogeneous photocatalytic removal of hazardous compounds from water and air*. National Renewable Energy Laboratory
- Casbeer, E., Sharma, V. K., & Li, X.-Z. (2012). Synthesis and photocatalytic activity of ferrites under visible light: a review. *Separation and Purification Technology*, 87, 1–14.
- Chala, S., Wetchakun, K., Phanichphant, S., Inceesungvorn, B., & Wetchakun, N. (2014). Enhanced visible-light-response photocatalytic degradation of methylene blue on Fe-loaded BiVO_4 photocatalyst. *Journal of Alloys and Compounds*, 597, 129–135.
- Derbal, A., Omeiri, S., Bouguelia, A., & Trari, M. (2008). Characterization of new heterosystem $\text{CuFeO}_2/\text{SnO}_2$ application to visible-light induced hydrogen evolution. *International Journal of Hydrogen Energy*, 33, 4274–4282.
- Eng, Y. Y., Sharma, V. K., & Ray, A. K. (2010). Photocatalytic degradation of nonionic surfactant, Brij 35 in aqueous TiO_2 suspensions. *Chemosphere*, 79(2), 205–209.
- Fogler, S. H. (2005). *Elements of chemical reaction engineering, 4th Edition*. Prentice-Hall.
- Ghomi, A. B., & Ashayeri, V. (2012). Photocatalytic efficiency of CuFe_2O_4 by supporting on clinoptilolitedecolorization of acid red 206 aqueous solutions. *Iranian Journal of Catalysis*, 2(3), 135–140.
- Kumar, V., Masudy-Panah, S., Tan, C. C., Wong, T. K. S., Chi, D. Z., & Dalapati, G. K. (2013). *Copper oxide based low cost thin film solar cells. Nano-electronics conference (INEC)* (pp. 443–445). Singapore: IEEE.
- Laurie, V. F., & Waterhouse, A. L. (2006). Oxidation of glycerol in the presence of hydrogen peroxide and iron in model solutions and wine. Potential effects on wine color. *Journal of Agricultural and Food Chemistry*, 54, 4668–4673.
- Liu, R., Yoshida, H., Fujita, S., & Arai, M. (2014). Photocatalytic hydrogen production from glycerol and water with $\text{NiO}_x/\text{TiO}_2$ catalysts. *Applied Catalysis B: Environmental*, 144, 41–45.
- Melo, M. O., & Silva, L. A. (2011). Visible light-induced hydrogen production from glycerol aqueous solution on hybrid Pt-CdS- TiO_2 photocatalysts. *Journal of Photochemistry and Photobiology A: Chemistry*, 226(1), 36–41.
- Qadariyah, L., Machmudah, S., Sasaki, M., & Goto, M. (2011). Degradation of glycerol using hydrothermal process. *Bioresource Technology*, 102(19), 9267–9271.
- Quispe, C. A. G., Coronado, C. J. R., & Carvalho, J. A., Jr. (2013). Glycerol: production, consumption, prices, characterization and new trends in combustion. *Renewable and Sustainable Energy Reviews*, 27, 475–493.
- Shahid, M., Jingling, L., Ali, Z., Shakir, I., Warsi, M. F., Parveen, R., & Nadeem, M. (2013). Photocatalytic degradation of methylene blue on magnetically separable MgFe_2O_4 under visible light irradiation. *Materials Chemistry and Physics*, 139(2–3), 566–571.
- Sharma, V. K., & Chenay, B. V. (2005). Heterogeneous photocatalytic reduction of Fe (VI) in UV-irradiated titania suspensions: effect of ammonia. *Journal of Applied Electrochemistry*, 35(7–8), 775–781.
- Sharma, V. K., Burnett, C. R., Rivera, W., & Joshi, V. N. (2001). Heterogeneous photocatalytic reduction of ferrate (VI) in UV-irradiated titania suspensions. *Langmuir*, 17(15), 4598–4601.
- Sharma, V. K., Graham, N. J., Li, X. Z., & Yuan, B. L. (2010). Ferrate (VI) enhanced photocatalytic oxidation of pollutants in aqueous TiO_2 suspensions. *Environmental Science and Pollution Research International*, 17(2), 453–461.
- Shen, Y., Wu, Y., Xu, H., Fu, J., Li, X., Zhao, Q., & Hou, Y. (2013). Facile preparation of sphere-like copper ferrite nanostructures and their enhanced visible-light-induced photocatalytic conversion of benzene. *Materials Research Bulletin*, 48(10), 4216–4222.
- Tan, H. W., Aziz, A. R. A., & Aroua, M. K. (2013). Glycerol production and its applications as a raw material: a review. *Renewable and Sustainable Energy Reviews*, 27, 118–127.
- Vadivel, S., Vanitha, M., Muthukrishnaraj, A., & Balasubramanian, N. (2014). Graphene oxide-BiOBr composite material as highly efficient photocatalyst for degradation of methylene blue and rhodamine-B dyes. *Journal of Water Process Engineering*, 1, 17–26.
- Wade, J. (2005). *An investigation of $\text{TiO}_2\text{-ZnFe}_2\text{O}_4$ nanocomposites for visible light photocatalysis*. Florida USA: Msc Thesis University of South Florida.
- Yang, H., Yan, J., Lu, Z., Cheng, X., & Tang, Y. (2009). Photocatalytic activity evaluation of tetragonal CuFe_2O_4 nanoparticles for the H_2 evolution under visible light irradiation. *Journal of Alloys and Compounds*, 476(1–2), 715–719.
- Yang, F., Hanna, M. A., & Sun, R. (2012). Value-added uses for crude glycerol—a byproduct of biodiesel production. *Biotechnology Biofuels*, 5, 13.
- Zhu, Z., Li, X., Zhao, Q., Li, Y., Sun, C., & Cao, Y. (2013). Photocatalytic performances and activities of Ag-doped CuFe_2O_4 nanoparticles. *Materials Research Bulletin*, 48(8), 2927–2932.